International Journal of Applied Earth Observation and Geoinformation 38 (2015) 292–301

Contents lists available at ScienceDirect

International Journal of Applied Earth Observation and Geoinformation

journal homepage: www.elsevier.com/locate/jag

The Advanced Spaceborne Thermal Emission and Reflection Radiometer (ASTER) after fifteen years: Review of global products

Michael Abrams[a,*], Hiroji Tsu[b], Glynn Hulley[a], Koki Iwao[c], David Pieri[a], Tom Cudahy[d], Jeffrey Kargel[e]

[a] Jet Propulsion Laboratory/California Institute of Technology, Pasadena, USA
[b] Japan Space Systems, Tokyo, Japan
[c] National Institute of Advanced Industrial Science and Technology, Tsukuba, Japan
[d] CSIRO, Perth, Australia
[e] University of Arizona, Tucson, USA

ARTICLE INFO

Article history:
Received 15 January 2015
Received in revised form 21 January 2015
Accepted 22 January 2015

Keywords:
ASTER
Terra
Earth Observing System
Global data

ABSTRACT

The Advanced Spaceborne Thermal Emission and Reflection Radiometer (ASTER) is a 15-channel imaging instrument operating on NASA's Terra satellite. A joint project between the U.S. National Aeronautics and Space Administration and Japan's Ministry of Economy, Trade, and Industry, ASTER has been acquiring data for 15 years, since March 2000. The archive now contains over 2.8 million scenes; for the majority of them, a stereo pair was collected using nadir and backward telescopes imaging in the NIR wavelength. The majority of users require only a few to a few dozen scenes for their work. Studies have ranged over numerous scientific disciplines, and many practical applications have benefited from ASTER's unique data. A few researchers have been able to mine the entire ASTER archive, that is now global in extent due to the long duration of the mission. Six examples of global products are described in this contribution: the ASTER Global Digital Elevation Model (GDEM), the most complete, highest resolution DEM available to all users; the ASTER Emissivity Database (ASTER GED), a global 5-band emissivity map of the land surface; the ASTER Global Urban Area Map (AGURAM), a 15-m resolution database of over 3500 cities; the ASTER Volcano Archive (AVA), an archive of over 1500 active volcanoes; ASTER Geoscience products of the continent of Australia; and the Global Ice Monitoring from Space (GLIMS) project.

Introduction

The Advanced Spaceborne Thermal Emission and Reflection Radiometer (ASTER) is a 15-channel imaging instrument operating on NASA's Earth Observing Terra morning orbital platform since 1999 (Yamaguchi et al., 1998). ASTER was built and provided by Japan's Ministry of Economy, Trade, and Industry (METI). ASTER has three separate optical subsystems: the visible and near-infrared (VNIR) radiometer, acquiring images in 3 bands with a 15 m instantaneous field of view (IFOV), and an additional backward-looking band for stereo; the shortwave infrared (SWIR) radiometer, acquiring images in 6 bands with a 30 m IFOV; and the thermal infrared (TIR) radiometer, acquiring images in 5 bands with a 90 m IFOV (Fig. 1). ASTER acquires images in all bands with a swath width of 60 km. It orbits the earth in a sun-synchronous near-polar orbit, with an equator crossing time of 10:30am, and the daytime repeat visit interval is 16 days at the equator.

There are several constraints on ASTER operations and data acquisitions. The primary constraint on how much data ASTER can acquire is dictated by the amount of space ASTER is allocated on the Terra solid state recorders, since there is no direct broadcast capability for ASTER; all data are relayed through the Tracking and Data Relay Satellite System to ground stations, several times each day. The maximum average data rate allocated to ASTER, based on two-orbit average, is 8.3 Mbps, which corresponds to 8 min of full-mode daytime operation per orbit. Other constraints include dissipation of heat, available power, length of downlink windows, design limitations of instrument components, and ability to schedule observations with the ASTER instrument.

ASTER, because of its limited duty cycle, is scheduled every day for specific data collections. These collections are selected from all the pertinent requests that potentially could be observed on a given day. A data base has been assembled that contains different categories of requests to collect data. These fall into three categories:

* Corresponding author. Tel.: +1 8183540927.

http://dx.doi.org/10.1016/j.jag.2015.01.013
0303-2434/

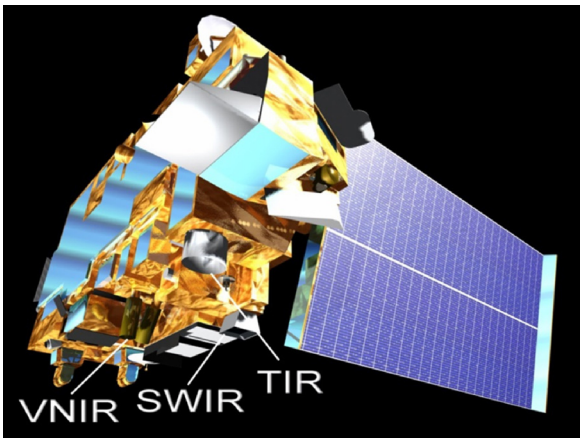

Fig. 1. Artist's rendition of the ASTER instrument on Terra.

(1) engineering data that are collected to monitor the instrument health and safety; (2) calibration data that are acquired as part of both vicarious and onboard calibration activities; (3) science data that are acquired to meet the science needs of the mission.

The science team developed the ASTER scheduler that automatically creates an observation schedule every day for upload and execution by ASTER. The data collection database is used to determine all possible submitted and requested observations that potentially could be observed on any given day. This always greatly exceeds the capabilities of ASTER to acquire data, so a triage is performed by the scheduler using prioritization parameters. We have additionally developed a system that allows manual modification of the one-day schedule to allow for emergency or urgent acquisitions (Duda and Abrams, 2012). These would include observations of natural disasters, such as volcanic eruptions, earthquakes, and hurricanes.

The three ASTER subsystems worked perfectly until April 2008, when the SWIR subsystem suffered a failure, probably due to decoupling of the detector from the cold finger. Since then, we have acquired VNIR and TIR data, both together during the daytime, and with only the TIR at nighttime.

ASTER delivers 12 data products to users, created on-demand. Besides the lower level radiance-at-the-sensor products for each subsystem, we make available calibrated geophysical variables, such as atmospherically corrected reflectance, kinetic temperature, emissivity, and digital elevation model. Any or all products can be ordered from any scene that has been acquired by ASTER and is stored in the archive. Since March 2000, ASTER has acquired over 2.8 million scenes. We have achieved nearly complete global coverage with all of the instruments and stereo acquisitions; for most areas we have up to hundreds of scenes at different times of year. A few perennially cloudy areas are missing from the archive.

In the last 15 years, the ASTER project has distributed over 800 Tb of data to the science community, representing over 30 million data products. The user community is global, with data going to users in over 120 countries. Our community includes government agencies, educational institutions and commercial vendors. A survey of the refereed published literature from the prior 3 year provides insight into some of the applications of ASTER data by a large and varied user community. ASTER data have been used for archaeological applications (Agapiou et al., 2014), urban heat island effects (Hu et al., 2012; Liu and Zhang, 2011), wetlands monitoring (Bortels et al., 2011), landslide susceptibility mapping (Choi et al., 2012), monitoring vineyards and tea quality (Ducati et al., 2014; Dutta et al., 2011), flood hazard mapping (Forkuo, 2011; Gichamo et al., 2012; Hanada and Yamazaki, 2012), riparian vegetation change and mangrove mapping (Kellogg and Zhou, 2014; Tamura, 2012), geologic mapping and resource exploration (Mars, 2014; Pour and Hashim, 2012; van der Meer et al., 2014, 2012), and mapping tree species diversity (Mutowo and Murwira, 2012).

These studies used a few to several dozen ASTER scenes. However, after 15 years of successful data acquisition, the ASTER data archive contained sufficient scenes to allow global data sets to be extracted. Several research teams have produced continental and global products using the massive archive of ASTER data. The rest of this article describes six of these that have been released in the last few years: the ASTER Global Digital Elevation Model (GDEM), the ASTER Emissivity Database (ASTER GED), the ASTER Global Urban Area Map (AGURAM), the ASTER Volcano Archive (AVA), ASTER Geoscience products, and the Global Ice Monitoring from Space (GLIMS) project.

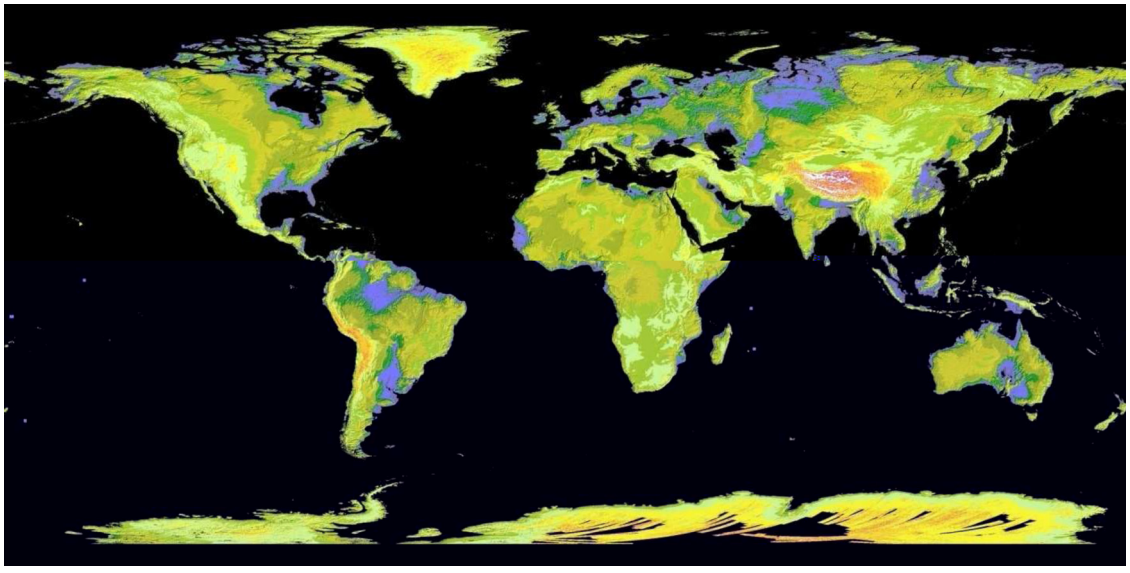

Fig. 2. ASTER GDEM, shaded relief version, with color-coded elevations; white is highest, red and orange next, yellows and greens next, purple and black lowest. (For interpretation of the references to color in this figure legend, the reader is referred to the web version of this article.)

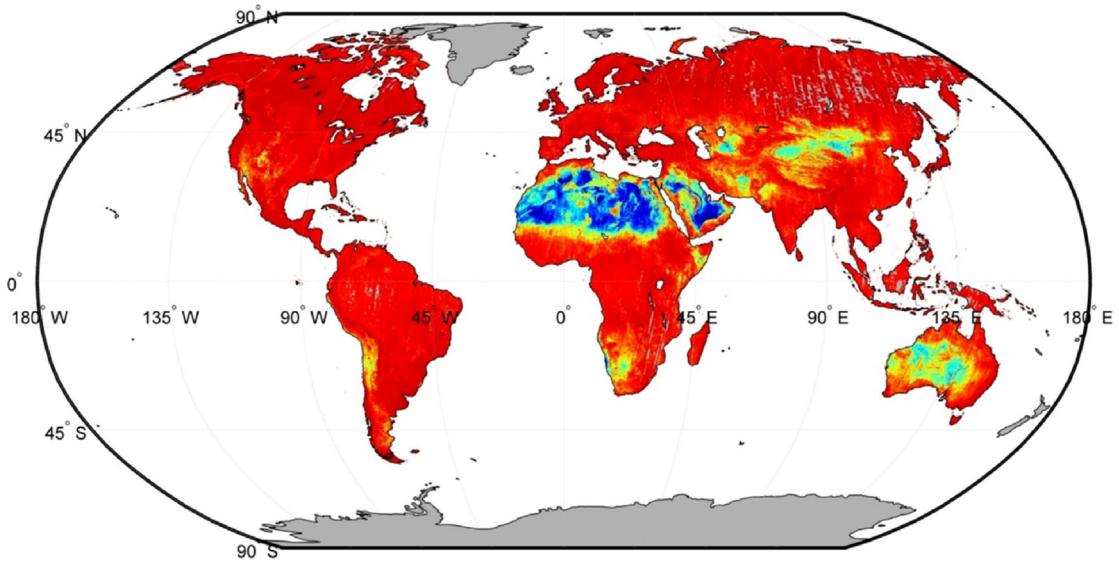

Fig. 3. ASTER GED for earth's land surfaces for band 12. Higher emissivity values are red, low are blue. The Sahara and Rub al'Khali exhibit the lowest values due to quartz absorption band. (For interpretation of the references to color in this figure legend, the reader is referred to the web version of this article.)

ASTER Global Digital Elevation Model (GDEM)

On June 29, 2009 the Ministry of Economy, Trade, and Industry (METI) of Japan and the U.S. National Aeronautics and Space Administration (NASA), jointly released Version 1 of the global digital elevation model (GDEM) of the Earth's land surface (Fig. 2), derived from 1.7 million images acquired by ASTER (Abrams et al., 2010). The ASTER GDEM is the most up-to-date, high spatial resolution, complete digital topographic data set of the Earth available at no cost to the public, covering the global land surface from 83°N to 83°S latitude. In 2007 the GDEM was offered by METI and NASA to the Group on Earth Observations (GEO) at the Summit of Ministers in Capetown, South Africa, and accepted as a contribution to the Global Earth Observing System of Systems (GEOSS) to serve societal needs.

Prior to the release of the ASTER GDEM, the most complete DEM available to the public was the Shuttle Radar Topography Mission (SRTM) data set (Farr and Kobrick, 2000; Farr et al., 2007). SRTM was a joint mission of NASA, German Aerospace Center, and the National Geospatial-Intelligence Agency. The SRTM data were created using interferometric processing of *L*-band synthetic aperture radar (SAR) data. The SRTM DEM is a surface model, with canopy, as is the ASTER GDEM. The SRTM data were released to the public at 90 m postings for areas outside the U.S. (vs. 30 m for GDEM), and 30 m postings for the US and its territories. The SRTM DEM covers the Earth from 60°N to 57°S latitude, thus missing the land masses north of 60° (Greenland; northern Canada, Europe, Asia, and Alaska) and Antarctica (that are covered by GDEM).

GDEM was produced from the entire 1.7 million scene ASTER archive. In addition to VNIR band 3 acquiring a nadir-look, there is a backward-looking telescope operating in the same spectral range. Every time there is a VNIR data acquisition, a stereo pair is collected. The backward-looking and nadir visible bands have a 28° look angle, thus giving a base-to-height ratio of 0.6. The pixel size of the visible and near infrared bands (and the stereo band) is 15 m. Standard stereocorrelation was used to produce individual scene models at 30 m postings. Cloud screening and quality control were applied before stacking and averaging elevations on a per pixel basis (Fujisada et al., 2012). The resulting data were partitioned into 22,600 $1 \times 1^{\circ}$ tiles.

Prior to their decision to release the GDEM, NASA and METI, in cooperation with the U.S. Geological Survey (USGS), the Earth Remote Sensing Data Analysis Center (Tokyo, Japan), and other collaborators, conducted extensive preliminary validation and characterization studies of the ASTER GDEM. For a discussion of these and additional GDEM accuracy assessment and characterization results, please see the "ASTER Global DEM Validation Summary Report" (ASTER Global Validation Summary Report, 2006).

A second version of the GDEM was released in October, 2011. In addition to adding 200,000 new images to the stereo-generation process, several artifacts and anomalies were corrected, and the overall accuracy was improved. A second validation and assess-

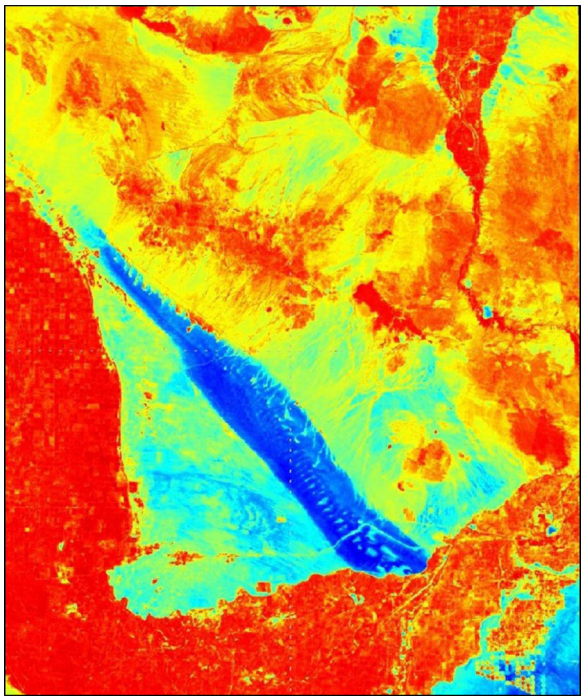

Fig. 4. $1 \times 1^{\circ}$ tile of ASTER GED for TIR band 12 (9.1 μ) over an area of southeastern California. Crests and troughs of the Algodones dunes are dark blue (low emissivity) due to the quartz absorption band, while vegetation over agricultural regions of Imperial Valley (western edge) results in higher emissivities (red). (For interpretation of the references to color in this figure legend, the reader is referred to the web version of this article.)

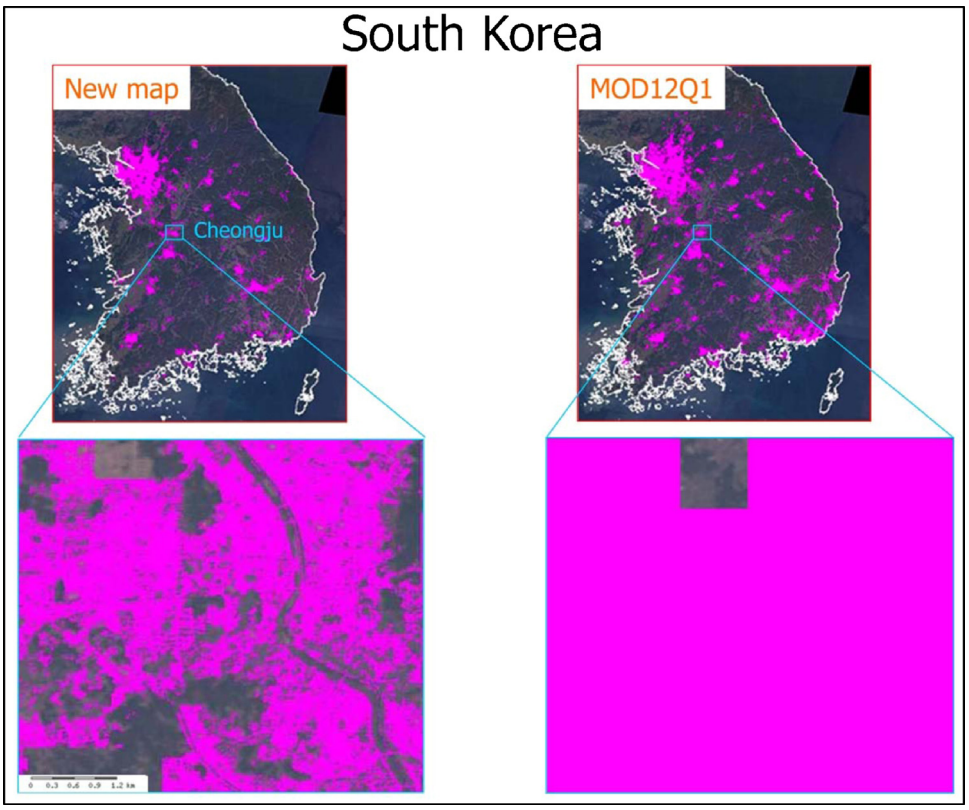

Fig. 5. AGURAM map for Cheongju, South Korea at 15 m resolution, compared with MODIS MOD12Q1 product at 1 km resolution. Urban areas are identified in magenta color. (For interpretation of the references to color in this figure legend, the reader is referred to the web version of this article.)

ment of accuracy were performed prior to release. The full report was posted on the distribution websites so that users would fully understand the characteristics of the GDEM data. As of September, 2014, over 29,000,000 GDEM tiles have been downloaded by users. In late 2015, Version 3 of the GDEM will be released. This version will include a global water body mask and data planes identifying the water body as ocean, lake or river. It is anticipated that this version will also be registered into the GEO Data Portal.

ASTER Global Emissivity Database (GED)

The Earth emits energy at thermal wavelengths, beyond the range of human visual sense, and that energy is a function of the temperature and the emissivity of the surface. The surface emissivity is an intrinsic property of the surface, primarily depends on surface composition, and is a gauge of the efficiency of a surface in radiating thermal energy in comparison to that of a blackbody at equivalent wavelengths. As the surface composition changes through, for example, land cover land use change, so does the surface emissivity. The emissivity is independent of the surface temperature, which varies with solar irradiance and local weather conditions. The emissivity of most natural Earth surfaces for ASTER's TIR wavelength ranges between ~0.65 and close to 0.99. Narrowband emissivities less than 0.85 are typical for most desert and semi-arid areas due to the strong quartz absorption feature, whereas the emissivity of vegetation, water and ice cover are generally greater than 0.95 and spectrally flat in the 8–12 μm range.

In land surface temperature (LST) modeling, knowledge of the surface emissivity is critical for accurately recovering the LST, a key climate variable in many scientific studies from climatology to hydrology and modeling the greenhouse effect. By inverting the Planck function and simulating a radiative transfer method for estimating LST, it can be shown that an emissivity error as little as 0.01 (1.0%) corresponds to a surface temperature error of ~0.6 K for a material at 300 K and a wavelength of 11 μm. The impact of emissivity errors on LST is larger for split-window algorithms, and depending on the water vapor content, are on average ~0.7 K for a band emissivity uncertainty of 0.005 (0.5%) (Galve et al., 2008).

Hulley and Hook (2009, 2011) have produced a Global Emissivity Database (GED) (Fig. 3), using the entire ASTER TIR archive for each of ASTER's 5 TIR bands. The ASTER GED products (Fig. 4) are output as $1^\circ \times 1^\circ$ tiles at 100-m or 1-km spatial resolution (nominal) and include the mean emissivity and standard deviation for all 5 ASTER thermal infrared bands, mean land surface temperature (LST) and standard deviation, a re-sampled ASTER GDEM, land-water mask, mean normalized difference vegetation index (NDVI) and standard deviation, latitude, longitude, and observation count.

The ASTER GED data are used by other instrument projects (such as the Atmospheric Infrared Sounder [AIRS], Moderate Resolution Imaging Spectrometer [MODIS] (Hulley et al., 2012), and the Tropospheric Emission Spectrometer [TES]) for validation, and as inputs to atmospheric composition retrievals. The surface emissivity is an unknown background for these TIR instruments. Knowing the emissivity of the surface materials allows a significant improvement in retrieval of atmospheric water vapor and atmospheric gas concentrations.

ASTER Global Urban Area Map (AGURAM)

Japan's National Institute of Advanced Industrial Science and Technology (AIST) has developed the AIST/ASTER Global Urban Area Map (AGURAM), a global urban settlement map with spatial resolution of 15 m (Fig. 5). It was developed with surface reflectance data acquired from ASTER's VNIR bands and various GIS data, such as existing MODIS coarse-resolution land cover maps and ASTER DEMs. The AGURAM was developed for 3374 cities of the world

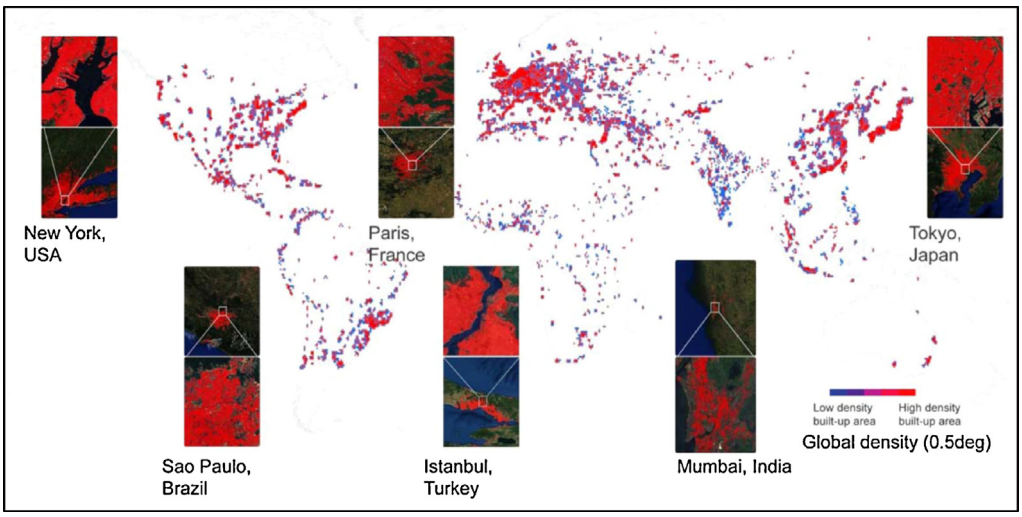

Fig. 6. AIST/ASTER Global Urban Area Map is a web-based mapping project using ASTER VNIR data to map urban areas at 15 m resolution for 3374 cities world-wide with populations greater than 100,000.

with populations of more than 0.1 million people using 11,802 scenes of ASTER/VNIR data acquired between January 2000 and March 2008 (Fig. 6).

The data processing system was developed on a grid computing system, GEO Grid, operated by AIST (Yamamoto et al., 2006). An automated algorithm using a combination of learning with local and global consistency (LLGC) and logistic regression (Miyazaki et al., 2012) was applied to development of the AGURAM. Accuracy of the AGURAM is rated as 0.670 for overall accuracy, 0.345 for kappa coefficient. This is better than or similar to MODIS' urban product MOD12Q1 with accuracies of 0.675 for overall accuracy and 0.300 for kappa coefficient; and the Global Rural-Urban Mapping Project (GRUMP) product with accuracy of 0.611 for overall accuracy and 0.121 for kappa coefficient. The AGURAM is available at GEO Grid WebGIS (http://maps.geogrid.org/examples/basemap/).

There are two existing urban extent maps, both at 1 km spatial resolution: MODIS' MOD12Q1 product, and the Global Rural-Urban Mapping Project (GRUMP) based mostly on nighttime light imagery. AGURAM is a two-orders-of-magnitude improvement with its 15 m spatial resolution. This unique data base has global applications including environmental assessment of CO_2 emissions; and regional applications including prediction of damage from disasters, socio-economic analyses of urban formation and growth, and environmental impacts of urban growth.

ASTER Volcano Archive (AVA)

The ASTER Volcano Archive (AVA; http://ava.jpl.nasa.gov) is the world's largest dedicated archive of web-accessible volcano images, and uniquely provides capability to inventory and monitor the geomorphic, geologic, physical, and chemical properties, processes, and related activity states of volcanoes globally (Pieri and Abrams, 2004; Pieri and Buongiorno, 2010). Such insights and systematic data include the spectral signatures and operative meso-scale processes for volcanic emissions (e.g., eruption columns and plumes), as well as for surficial deposits (e.g., lava flows, pyroclastic flows), eruption precursor phenomena, and associated geo-botanical damage (e.g., SO_2 generated acid rain damage, CO_2 root suffocation).

AVA has significantly improved the global monitoring and access to archival ASTER image data of the Earth's 1500+ active volcanoes, providing prompt on-line access to approximately 165,000 full resolution day and night ASTER images acquired over the mission lifetime since 2000 (in geo-referenced jpeg format). We have responded to approximately 20 million web data requests from over 150,000 unique users over the last four years, and have constructed a number of volcano-specific ASTER HDF archives, some in an emergency request mode (e.g., Democratic Republic of the Congo; Vanuatu). We continue to operate AVA to provide ASTER data access to the general public and the volcanology community, and to conduct research utilizing this unique data compilation.

At the heart of AVA is an archive of continuously updated full spatial resolution jpeg color composites of all ASTER multispectral bands for all of our volcanoes: VNIR, SWIR (up through 2008), and TIR images, as well as ASTER GDEM data for each volcano. The concatenation of such data in an easily accessible format is proving to be enormously useful in organizing the multi-spectral geological analysis of a particular volcano (i.e., Amici et al., 2013).

We are in the process of adding ASTER emissivity maps for all volcanoes, as well as alteration zone maps and potential lahar trajectories vs. population maps for roughly two thirds of the archive (in collaboration with the US Geological Survey). In addition, we are compiling eruption image sequences of ASTER data (with MODIS and other TERRA, AQUA, and AURA data supplements) for all eruptions during the ASTER mission lifetime, based on over 35,000 US Air Force Weather agency volcanic activity bulletins, and Smithsonian Global Volcanism Program bulletins, with links to the original data.

To expand both the temporal observation frequency for this set of active volcanoes, and to extend our temporal range, we are adding Landsat data for each of our volcanoes, over the entire life of the Landsat Program (1972-present). The data are presented in image processing formats comparable to our ASTER image data, and comprise an entirely complementary and synergistic data set. To date, we have ingested into AVA, all available Landsat 8 data, and the ingestion of Landsat 7 data is underway. In addition, we will add the much smaller, but spectrally comprehensive NASA EO-1 data set (e.g., Hyperion and the Advanced Land Imager [ALI] data sets). Taken together, the data sets of expanded AVA will comprise the most comprehensive compilation of orbital high spatial resolution volcano image data ever assembled. All our data are compatible with, and can thus be directly downloaded and displayed within, the Google Earth™ application (i.e., kmz-enabled). This provides an enormously useful tool for browsing and analyses. For example, comprehensive time series data for a particular volcano can be used to discern activity patterns that may reveal eruption precursor

Fig. 7. Landing page for ASTER Volcano Archive (AVA) web site. A unique archive of remote sensing data, geophysical maps, and analyses is available for 1546 recently active volcanoes.

phenomena (e.g., Buongiorno et al., 2013). The collating of ASTER and other data in an easy-to-access time series format is a significant contribution of the AVA to the volcanological community.

Further expansion plans for the AVA include the addition of relevant ancillary data including radar image and deformation data, hand-held imagery from the International Space Station, and selected volcanic province mosaics (e.g., Snake River Plain, Afar Rift). We are also implementing new algorithms developed at JPL for enhanced detail discrimination, better snow-ice-cloud discrimination, sulfur dioxide detection, and thermal anomaly detection.

At JPL, our scientific research, enabled by the compilation of AVA, involves investigations of the fundamental relationship between the onset of gas emission and related thermal anomalies, and subsequent eruptions; the relationship between erosion rates and volcano deposit resurfacing rates in the context of long-term (e.g., ~10–100 year) eruption probabilities for active volcanoes with

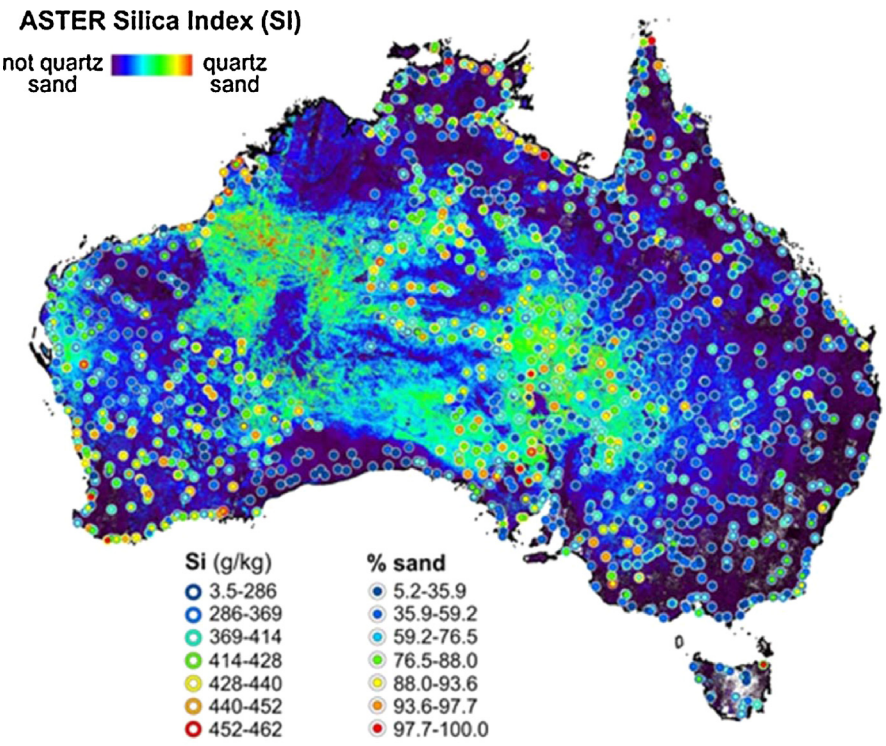

Fig. 8. Silica index map (together with field validation data) is one of 17 ASTER Australia Geoscience products freely available through the CSIRO Data Portal.

repose periods of hundreds of years; as well as conducting systematic in situ sampling of volcanogenic SO_2 and ash emissions for calibration and validation of gas and solid aerosol meso-scale detection and transport models. Our overall goal is to continue and improve the access to, and utilization of, our comprehensive and unique ASTER volcano data archive, especially as expanded to include other relevant NASA data, and to use it to conduct systematic volcanological analyses at regional and global scales. The GUI (http://ava.jpl.nasa.gov/) has been designed for both the science community and the public at large (Fig. 7).

ASTER Geoscience products

The overall objective of CSIRO's Australian ASTER initiative is to provide national, public, web-accessible, GIS-compatible ASTER geoscience maps (chiefly, mineral groups) of Australia, suitable for mapping from the continental-scale down to 1:50,000 prospect-scale. To that end, all of the 35,000 ASTER images over Australia were acquired; approximately 3500 were used to construct the mosaic of Australia.

The scenes were pre-processed, and masks were applied to remove complicating effects (clouds, green vegetation, deep shadow, water). The data were converted to calibrated reflectance with the assistance of limited Hyperion data (Caccetta et al., 2013). Mosaicking involved precision navigation and smoothing/normalization of overlapping edges. The 14 channels of ASTER VNIR, SWIR and TIR data were used as inputs to various mathematical transformations and logical operators based on analyses of laboratory spectral reflectance and emission measurements (Laukamp et al., 2012).

There are seventeen Version 1 Geoscience products, including fourteen from ASTER's nine visible, near-infrared (VNIR) and shortwave infrared (SWIR) "reflected" bands as well as three from ASTER's five thermal infrared (TIR) bands. Products include: false color composite, green vegetation content, CSIRO "regolith" ratios, ferric oxide content, ferrous iron content, opaques, ALOH group (clay) content, ALOH group composition, kaolin and "advanced argillic", Fe–OH group content, MgOH/carbonate group, MgOH group composition, ferrous iron content in MgOH, ferric iron content in MgOH, silica index (Fig. 8), quartz index, and gypsum index. The continental mosaic of geoscience data products was input into the CSIRO Data Access Portal, from which it can be accessed and downloaded, in part or in whole (CSIRO Data Acess Portal, 2014).

These new ASTER Geoscience products range in their application from local to continental scales, and their uses include mapping of soils for agricultural and environmental management, such as estimating soil loss, dust management and water catchment modeling. These products are also useful for resource exploration, as they reveal mineralogy of parent rocks as well as superimposed alteration and weathering effects. Indeed the first gold discovery based on these data was announced on the Australian stock exchange in 2012.

In addition to their value for regional to prospect scale exploration and associated targeting, regional mineral resource exploration, the maps also show how mineralogy across the Australian continent has developed in response to climate, weathering, erosional and depositional processes. For example, the ferric oxide composition and AlOH composition products show that hematite and kaolinite, respectively, are developed over deeply weathered, thick, stable crust, such as the region spanning the Yilgarn Block in Western Australia to the Gawler Craton in South Australia. This deep weathering developed during the Cenozoic (45–10 Ma) during a time when the monsoonal belt was much further south than its present position in the tropics where deep weathering continues. This change in climate resulted in aridity across central Australia causing the formation of extensive sandy deserts, which are well mapped using the ASTER silica index product. A region of thin crust centered below the Great Australian Basin resulted in an overlying depression for much of the Phanerozoic where sediment has been deposited. This sediment is characterised by illite-montmorillonite clays and is well mapped using the ASTER Al-clay composition. Dr Cudahy's CSIRO team are now working on

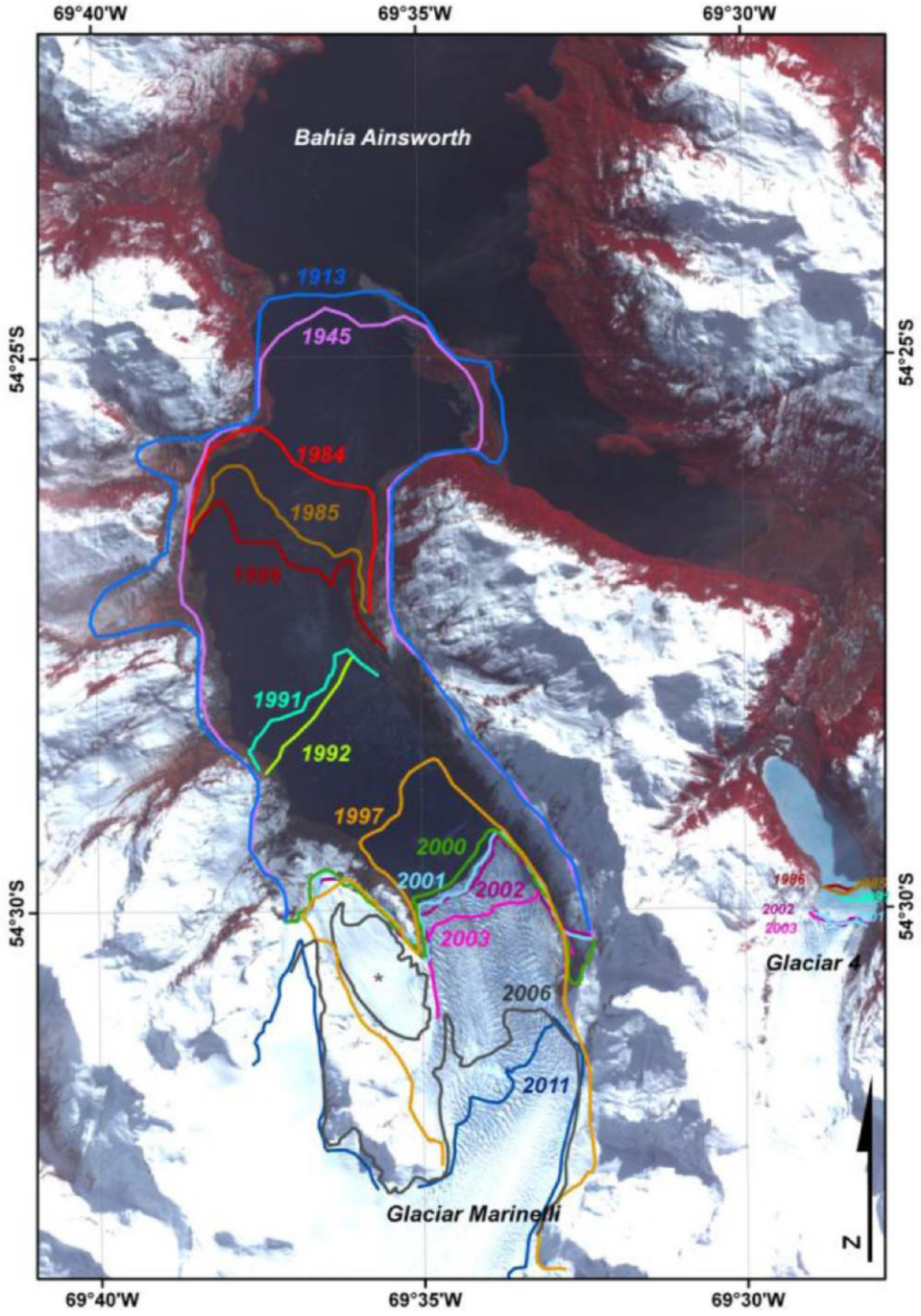

Fig. 9. Glaciar Marinelli in Chile showing progressive 15 km retreat of glacier front since 1913.

Version 2 ASTER Geoscience products, which includes removing the effects of green vegetation from the mineral content products. They are also working on two new Geoscience products, namely an integrated SWIR-TIR index that measures the proportion of clay-to-sand size materials, as well as an index sensitive to water, including water vapor and soil moisture.

Dr Cudahy and his CSIRO team are now extending and testing the universal applicability of these Version 2 ASTER geosciences products to other regions of the Earth, including parts of South America and China. The eventual goal is to produce global mineral maps for at least those areas where minerals are exposed, such as the world's extensive drylands, which are sensitive to climate change and anthropogenic effects that can cause the land degradation process of desertification.

Global Ice Monitoring from Space (GLIMS)

Global Land Ice Measurements from Space (GLIMS) is a project designed to monitor the world's glaciers primarily using data from optical satellite instruments, such as ASTER. GLIMS began as

an ASTER Science Team project. Through this connection, GLIMS guided the ASTER instrument team to acquire imagery of Earth's glaciers that is optimized (best season and instrument gain settings) for glacier monitoring. The GLIMS project has also put together a network of international collaborators who analyze imagery of glaciers in their regions of expertise. Analysis results include digital glacier outlines and related metadata, and can also include snow lines, center flow lines, hypsometry data, surface velocity fields, and literature references. Over 60 institutions across the globe are involved in GLIMS. The project is coordinated by principal investigator Dr. Jeffrey S. Kargel of the University of Arizona Department of Hydrology and Water Resources. The GLIMS Database (GGDB) and GLIMS web site are developed and maintained by the National Snow and Ice Data Center (NSIDC) in Boulder, Colorado, USA. Results from analysis done by the regional centers are sent for archive to the GGDB.

The GLIMS project also continues to aid the transfer of data to the GGDB from other databases. GLIMS web-based support tools are available at http://glims.colorado.edu/tools/ for data analysis, formatting and quality control.

A major output from the GLIMS project is a 33-chapter book on selected results from the GLIMS investigators (Kargel et al., 2014). An example from the book is found in chapter 28 by Bown and Rivera (2014). Their research team addressed a scientific gap by providing a full inventory for glaciers lying south of 54°S. A total of 1681 glaciers were delineated with an ice surface of 3300 km^2. A stunning example, among dozens of others showcased and described in the book, is Glaciar Marinelli (Fig. 9), with a history of 15 km retreat since 1913.

One recent major application of the GLIMS project is the Randolph Glacier Inventory (RGI 3.2), a global inventory of glacier outlines (National Center for Atmospheric Research Staff, 2013). It is supplemental to the GLIMS initiative. Production of the RGI was motivated by the forthcoming Fifth Assessment Report of the Intergovernmental Panel on Climate Change (IPCC AR5) and was being released initially with little documentation in view of the IPCC's tight deadlines during 2012. RGI is one of the most comprehensive and up-to-date inventories of world glaciers, containing 700,000 km^2 of glacier area. The glacier outlines can be combined with DEMs to give areas, area distributions and area-elevation distributions. The RGI is in the process of being integrated with the GGDB.

Discussion and conclusions

ASTER has been successfully acquiring images for 15 years on NASA's Terra satellite. Despite a limited duty cycle, ASTER has obtained global coverage of the entire earth's land surface, often archiving hundreds of images for an area, over the lifetime of the mission. While most users use a small number of ASTER images and data products for their research, several scientific teams have mined the data archive to assemble global data products. The six examples described here present unique global data sets that are used by numerous researchers, by other spaceborne instrument teams, by commercial enterprises, and by government policy makers. With a mission life expectancy of up to seven more years, ASTER on Terra will continue to obtain data for future users and new global uses.

In retrospect, the single most limiting factor in the mission design was the capacity of Terra's on-board solid state recorder. While we had access to the latest state-of-the art space-qualified hardware, the components were selected in the early 1990s, using technology designed in the 1980s. ASTER was given more than half the recording capacity on Terra; however that translated to an 8% average duty cycle, or about 500 images per day. The high instantaneous data rate from our 15 channels quickly filled up the recorder. As a result, we were unable to plan a global mapping mission; and in addition we had to create a complex data scheduling algorithm to prioritize each day's data acquisitions.

ASTER has unequivocally demonstrated the enormous value of multispectral shortwave infrared bands for surface composition mapping; and of multispectral thermal infrared bands for accurate surface temperature retrieval and surface composition mapping. Multiple SWIR bands are found on the WorldView-3 commercial satellite, launched in 2014. It offers very high spatial resolution, but provides a narrow field of view and only limited spatial sampling of the land surface. Multispectral TIR will be the focus of NASA's ECOSTRESS mission on the International Space Station. Its goal is to observe daily and seasonal changes in plant biophysics to model evapotranspiration, and has a limited sampling strategy during its one year of operation in 2019. NASA is investigating the Hyperspectral Infrared Imager (HyspIRI) mission that combines a Hyperspectral VNIR-SWIR instrument and a multispectral TIR instrument. It is currently in pre-Phase A funding and has no announced start date.

Acknowledgments

Work by Abrams, Hulley and Pieri was performed at the Jet Propulsion Laboratory, California Institute of Technology under contract with the National Aeronautics and Space Administration.

References

Abrams, M., Bailey, B., Tsu, H., Hato, M., 2010. The ASTER Global DEM. J. Am. Soc. Photogramm. Remote Sens. 20, 344–348.

Agapiou, A., Alexakis, D.D., Hadjimitsis, D.G., 2014. Spectral sensitivity of ALOS, ASTER, IKONOS, LANDSAT and SPOT satellite imagery intended for the detection of archaeological crop marks. Int. J. Digital Earth 7 (5), 351–372, http://dx.doi.org/10.1080/17538947.2012.674159.

Amici, S., Piscini, A., Buongiorno, M.F., Pieri, D., 2013. Geological classification of volcano Teide by hyperspectral and multispectral satellite data. Int. J. Remote Sens. 34 (9–10), 3356–3375.

ASTER Global Validation Summary Report. 2009. <https://lpdaac.usgs.gov/lpdaac/content/download/4009/20069/version/1/file/ASTER+GDEM+Validation+Summary+Report+-+FINAL+for+Posting+06-28-09.pdf>(viewed 15.09.14.).

Bortels, L., Chan, J.C.W., Merken, R., Koedam, N., 2011. Long-term monitoring of wetlands along the Western-Greek bird migration route using Landsat and ASTER satellite images: Amvrakikos Gulf (Greece). J. Nat. Conserv. 19 (4), 215–223, http://dx.doi.org/10.1016/j.jnc.2011.01.004.

Bown, F., Rivera, A., 2014. First glacier inventory in parts of Tierra del Fuego, Southern Chile, page 14. In: Kargel, J.S., Leonard, G.J., Bishop, M.P., Kääb, A., Raup, B.H. (Eds.), Select Chapter Highlights from the Book, Global Land Ice Measurements from Space, 2014. Springer–Praxis, Berlin, Heidelberg, p. 876 (17 pages).

Buongiorno, M.F., Pieri, D.C., Silvestri, M., 2013. Thermal analysis of volcanoes based on 10 years of ASTER data on Mt. Etna. In: Kuenzer, C., Dech, S. (Eds.), Thermal Infrared Remote Sensing: Sensors, Methods, Applications, Remote Sensing and Digital Image Processing. , p. 17, http://dx.doi.org/10.1007/978-94-007-6639-6-20.

Caccetta, M., Collings, S., Cudahy, T., 2013. A calibration methodology for continental scale mapping using ASTER imagery. Remote Sens. Environ. 138, 306–317.

Choi, J., Oh, H.-J., Lee, H.-J., Lee, C., Lee, S., 2012. Combining landslide susceptibility maps obtained from frequency ratio, logistic regression, and artificial neural network models using ASTER images and GIS. Eng. Geol. 124, 12–23, http://dx.doi.org/10.1016/j.enggeo.2011.09.011.

CSIRO Data Access Portal. 2014. <https://data.csiro.au/dap/landingpage?pid=csiro%3A6182>(viewed 20.09.14.).

Ducati, J.R., Sarate, R.E., Fachel, J.M.G., 2014. Application of remote sensing techniques to discriminate between conventional and organic vineyards in the Loire Valley, France. J. Int. Sci. Vigne Vin 48 (3), 135–144.

Duda, K., Abrams, M., 2012. ASTER satellite observations for international disaster management. Proc. IEEE 100, 2798–2811.

Dutta, R., Stein, A., Bhagat, R.M., 2011. Integrating satellite images and spectroscopy to measuring green and black tea quality. Food Chem. 127 (2), 866–874, http://dx.doi.org/10.1016/j.foodchem.2010.12.160.

Farr, T.G., Kobrick, M., 2000. Shuttle radar topography mission produces a wealth of data. Am. Geophys. Union Eos 81, 583–585.

Farr, T.G., et al., 2007. The shuttle radar topography mission. Rev. Geophys. 45, RG2004, http://dx.doi.org/10.1029/2005RG000183.

Forkuo, E.K., 2011. Flood hazard mapping using Aster image data with GIS. Int. J. Geom. Geosci. 1 (4), 932–950.
Gichamo, T.Z., Popescu, I., Jonoski, A., Solomatine, D., 2012. River cross-section extraction from the ASTER global DEM for flood modeling. Environ. Modell. Softw. 31, 37–46, http://dx.doi.org/10.1016/j.envsoft.2011.12.003.
Hanada, D., Yamazaki, F., 2012. Detection of flooded areas by the 2011 Tohoku earthquake tsunami using ASTER thermal infrared images. J. Jpn. Assoc. Earthquake Eng. 12 (6), 663–6672, http://dx.doi.org/10.5610/jaee.12.6-63.
Hu, D., Yang, L., Zhou, J., Deng, L., 2012. Estimation of urban energy heat flux and anthropogenic heat discharge using aster image and meteorological data: case study in Beijing metropolitan area. J. Appl. Remote Sens. 6, 63559, http://dx.doi.org/10.1117/1JRS.6.063559.
Fujisada, H., Urai, M., Iwasaki, A., 2012. Technical methodology for ASTER global DEM. IEEE Trans. Geosci. Remote Sens. 50 (10), 3725–3736.
Galve, J.A., Coll, C., Caselles, V., Valor, E., 2008. An atmospheric radiosounding database for generating land surface temperature algorithms. IEEE Trans. Geosci. Remote Sens. 46 (5), 1547–1557.
Hulley, G., Hook, S., 2009. The North American land surface emissivity database (NAALSED) Version 2. 0. Remote Sens. Environ. 112, 1967–1975.
Hulley, G.C., Hook, S.J., 2011. Generating consistent land surface temperature and emissivity products between ASTER and MODIS data for earth science research. IEEE Trans. Geosci. Remote Sens. 49 (4), 1304–1315, http://dx.doi.org/10.1109/tgrs.2010.2063034.
Hulley, G.C., Hughes, C.G., Hook, S.J., 2012. Quantifying uncertainties in land surface temperature and emissivity retrievals from ASTER and MODIS thermal infrared data. J. Geophys. Res.-Atmos. 117, D23113, http://dx.doi.org/10.1029/2012JD018506.
Kargel, J.S., Leonard, G.J., Bishop, M.P., Kaab, A., Raup, B. (Eds.), 2014. Global Land Ice Measurements from Space. Springer–Praxis, p. 876, An edited 33-chapter volume. ISBN: 978-3-540-79818-7.
Kellogg, C.H., Zhou, X.B., 2014. Impact of the construction of a large dam on riparian vegetation cover at different elevation zones as observed from remotely sensed data. Int. J. Appl. Earth Obs. Geoinf. 32, 19–34, http://dx.doi.org/10.1016/j.jag.2014.03.021.
Laukamp, C., Caccetta, M., Collings, S., et al., 2012. Continent-scale mineral information from ASTER multispectral satellite data, 2012 IEEE international geoscience and remote sensing symposium (IGARSS). In: Book Series: IEEE International Symposium on Geoscience and Remote Sensing, IGARSS, pp. 7553–7556.
Liu, L., Zhang, Y., 2011. Urban heat island analysis using the landsat TM data and ASTER data: a case study in Hong Kong. Remote Sens. 3 (7), 1535–1552.
Mars, J.C., 2014. Regional mapping of hydrothermally altered igneous rocks along the Urumieh–Dokhtar, Chagai, and Alborz Belts of western Asia using Advanced Spaceborne Thermal Emission and Reflection Radiometer (ASTER) data and interactive data language (IDL) logical operators; a tool for porphyry copper exploration and assessment. In: Scientific Investigations Report. U. S. Geological Survey, Reston, VA, pp. 36, http://dx.doi.org/10.3133/sir201050900.
Miyazaki, H., Shao, X., Iwao, K., Shibasak, R., 2012. An automated method for global urban area mapping by integrating ASTER satellite images and GIS data. IEEE J. Sel. Top. Appl. Earth Obs. Remote Sens. 6 (2), 1004–1019.
Mutowo, G., Murwira, A., 2012. Relationship between remotely sensed variables and tree species diversity in savanna woodlands of Southern Africa. Int. J. Remote Sens. 33 (20), 6378–6402, http://dx.doi.org/10.1080/01431161.2012.687472.
National Center for Atmospheric Research Staff (Eds.). 2013. The Climate Data Guide: Randolph Glacier Inventory data base of global glacier outlines. Retrieved from: <https://climatedataguide.ucar.edu/climate-data/randolph-glacier-inventory-data-base-global-glacier-outlines>(last modified 20.08.13.).
Pieri, D., Abrams, M., 2004. ASTER watches the world's volcanoes: a new paradigm for volcanological observations from orbit. J. Volcanol. Geotherm. Res. 135 (1-2), 13–28.
Pieri, D., Buongiorno, M.F., 2010. Long term observations of active volcanoes: orbital missions and growing remote sensing archives. In: Proceedings of the 3rd International Symposium on Recent Advances in Quantitative Remote Sensing (RAQRS), 27 September–01 October, Torrent (Valencia), Spain.
Pour, A.B., Hashim, M., 2012. The application of ASTER remote sensing data to porphyry copper and epithermal gold deposits. Ore Geol. Rev. 44, 1–9, http://dx.doi.org/10.1016/j.oregeorev.2011.09.009.
Tamura, M., 2012. Mapping mangrove forests using a short-wave-infrared band and a digital elevation model. J. Remote Sens. Soc. Jpn. 32 (4), 221–231, http://dx.doi.org/10.11440/rssj.32.221.
van der Meer, F., Hecker, C., van Ruitenbeek, F., van der Werff, H., de Wijkerslooth, C., Wechsler, C., 2014. Geologic remote sensing for geothermal exploration: a review. Int. J. Appl. Earth Obs. Geoinf. 33, 255–269, http://dx.doi.org/10.1016/j.jag.2014.05.007.
van der Meer, F.D., van der Werff, H.M.A., van Ruitenbeek, F.J.A., Hecker, C.A., Bakker, W.H., Noomen, M.F., van der Meijde, M., Carranza, E.J.M., de Smeth, J.B., Woldai, T., 2012. Multi- and hyperspectral geologic remote sensing: a review. Int. J. Appl. Earth Obs. Geoinf. 14 (1), 112–128, http://dx.doi.org/10.1016/j.jag.2011.08.002.
Yamaguchi, Y., Kahle, A., Tsu, H., Kawakami, T., Pniel, M., 1998. Overview of Advanced Spaceborne Thermal Emission and Reflection Radiometer (ASTER). IEEE Trans. Geosci. Remote Sens. 36, 1062–1071.
Yamamoto, N., Nakamura, R., Yamamoto, H., et al., 2006. GEO grid: grid infrastructure for integration of huge satellite imagery and geoscience data sets. Proceedings of the 6th IEEE International Conference on Computer and Information Technology, 75.